Journal of Porous Materials (2024) 31:1029–1041
https://doi.org/10.1007/s10934-024-01584-x

Metal-containing zeolite composites with separated phases as catalysts for hydroisomerization of linear hexane

Yuliya G. Voloshyna[1] · Olexandra P. Pertko[1] · Angela V. Yakovenko[1] · Volodymyr A. Povazhnyi[1] · Lyubov K. Patrylak[1]

Accepted: 26 February 2024 / Published online: 12 March 2024

Abstract
In this work, composite catalytic systems of natural mordenite and synthetic MFI-type zeolite containing Pd and Ni nanoparticles (0.5–1.5% by weight in total) were prepared by mechanical mixing (1:1), optionally with the addition of α- or γ-Al_2O_3 as a binder. The samples were examined using IR spectroscopy, X-ray diffractometry, transmission electron microscopy, low-temperature nitrogen ad(de)sorption, and tested in the model reaction of n-hexane hydroisomerization in a micro-pulse mode to determine the effect of composition on the peculiarities of linear alkane transformation. It has been shown that in the obtained catalytic systems, modifications of aluminum oxide used as a binder affect the effectiveness of catalysts in the conversion of n-hexane. This is explained by the different dispersity of α- and γ-Al_2O_3 particles, which causes differences in the characteristics of the porous structure of the obtained composites and, in turn, different accessibility of their active sites. In this respect, α-Al_2O_3 proved to be better than γ-Al_2O_3. The highest effectiveness in the formation of hexane isomers in general, as well as dimethyl branched isomers, was demonstrated by the sample possess the maximum concentration of Brønsted acid sites and the highest Brønsted/Lewis ratio. Synergy between the two zeolite components in the formation of isomers has been found out, which was more effective in samples with an isotropic distribution of zeolite phases. The synergetic effect is explained by the productive mutual influence of metal phases included in the zeolite.

Keywords Natural mordenite · MFI-type zeolite · Aluminum oxides · Bi-zeolite composite catalysts · Porosity · Alkane hydroisomerization

1 Introduction

Traditionally, zeolites are widely used as a basis of catalysts for various types of reactions. One of the ways to increase their effectiveness is to change the properties of the zeolite component. In particular, different combinations of zeolites can be used. The combination of zeolites of various types and other materials into composite catalytic systems allows of optimal use of their structural and acid-base characteristics, thus regulating the content and strength of active sites and their availability in the resulting material, which opens broad prospects for the use of such systems in catalysis.

Composite materials are an example of such bi-zeolite systems. In the literature, various methods of synthesizing composites are described, one of which is co-crystallization. The production of composites in this way by varying the conditions during synthesis is possible only for a small number of zeolites with similar structures, such as FAU (X) and LTA, MFI and MEL, FAU and EMT, STF and SFF [1], and BEA and MOR [2, 3]. Instead, by combining structure-directing agents and/or zeolite grains as a seed, or using them sequentially, as well as by recrystallization of zeolite under hydrothermal conditions in the presence of a structure-directing agent, it is possible to obtain composites of structures of a wider range: MFI and MEL [4], MWW and FER [5, 6], MFI and FAU [7–9], MOR and MFI [10], MFI and CHA [11]. In co-crystallized zeolites, the phases can be spaced much closer than in a physical mixture, and some parts of the composite can be fused [6], resulting in improved acidic properties and catalytic activity of the

✉ Yuliya G. Voloshyna
yule.v444@gmail.com

[1] V.P. Kukhar Institute of Bioorganic Chemistry and Petrochemistry of the NAS of Ukraine, Kyiv, Ukraine

composites compared to individual pure phases [5] or their mechanical mixtures [2, 3, 12]. However, composites can also demonstrate intermediate behavior between the two forming structures in various reactions [4, 10, 11].

Many publications are devoted to the synthesis and study of the properties of composites with a core-shell structure containing various combinations of zeolites: FAU/BEA [13], MOR/BEA [14], MOR/MFI [15], ZSM-5/SAPO-34 (/SAPO-5, /SAPO-11) [16–19], etc. They are obtained by a two-step procedure that involves the synthesis of zeolite, whose crystallites serve as the core, and the overgrowth of the shell onto modified core crystallites. Due to their optimized acid and porosity characteristics, such composites also demonstrate full or partial advantage in a number of catalytic reactions: oil refining [13], conversion of 1, 3, 5-TMB [14], conversion of methanol to aromatics [16], aromatization of isobutane [18].

As a component in composites of various structures, including those prepared by mechanical mixing [20], mesoporous materials are widely used: oxides Al_2O_3–SiO_2 [21], hierarchical MCM-41 [22, 23], silica SBA-15 [24, 25]. Such composites are useful in reactions involving macromolecules, as they are characterized by shape-selectivity and the ability to ease the diffusion of target products from the channels, which simultaneously prevents the formation of coke deposits and prolongs the stable operation of the catalyst. The positive effect of using micro-mesoporous composites as catalysts was noted in the reactions of catalytic cracking of crude oil [21] and soybean oil [20], liquid-phase alkylation of benzene with long-chain olefins [22], conversion of heavy reformate to xylenes [23], nitration of benzenes [24], and hydroisomerization of n-hexadecane [25]. Composite materials can contain a variety of natural minerals along with the zeolite component, which significantly reduces the final cost of the catalyst [26, 27]. Using natural materials, effective and inexpensive composite FCC catalysts [12, 28] and catalysts for glucose transformation into 5-hydroxymethylfurfural [29] based on kaolin, bentonite/zeolite-P catalyst of high stability for transesterification of palm oil [30], perlite- and obsidian-based catalysts for the process of 1,1-diethoxyethane production from acetaldehyde and ethanol [31] were developed.

As follows from the analysis of literature sources, composite catalytic systems obtained by mechanical mixing of components are relatively poorly studied, but often approach the effectiveness of "true" composites [7, 11, 17, 19]. In addition, the mechanical mixing method makes it possible to combine zeolite components modified with different metals, which expands the possibilities for adjusting the properties of the composite. At the same time, the procedures for the synthesis of "true" zeolite composites are quite complex. In view of this, the aim of this work was to evaluate the catalytic action of metal-containing bi-zeolite composites with separated phases prepared by mechanical mixing in the conversion of linear alkanes. The hydroisomerization of n-hexane was chosen as a model reaction.

2 Experimental

2.1 Catalyst preparation

The choice of zeolite components for obtaining composites was based on the analysis of the results of previous studies [32–35]. Synthetic MFI type powdered zeolite with a ratio of $SiO_2/Al_2O_3 = 41$ and a static capacity for water and heptane vapors of 0.07 cm^3/g and 0.18 cm^3/g, respectively, was used as a base of the first component. A base for the second component was Transcarpathian mordenite-containing rock with a mordenite content of 72 wt%, a ratio of $SiO_2/Al_2O_3 = 9.5$, and a molar content (mmol/g): Na_2O – 0.18, K_2O – 0.22, CaO – 0.52, Al_2O_3 – 1.16, SiO_2 – 10.97, H_2O – 6.1.

The H-form of the zeolites was obtained by calcining the NH_4-form at 873 K for 3 h. To do this, first, cations of the initial forms of zeolites (0,5–1 mm fraction) were exchanged for NH_4^+ cations from a 3 mol/L NH_4NO_3 solution. Then, the MFI-component was obtained by introducing 1 wt% Pd into the HMFI zeolite, and the MOR-component was obtained by introducing 2 wt% Ni into the dealuminated H-form of rock (HR). Metals were introduced by the incipient wetness impregnation technique. Air-dry zeolite samples were dehydrated in a muffle furnace (653 K, 2 h), impregnated with a calculated amount of $PdCl_2$ solution in 0.5 mol/L HCl or $Ni(NO_3)_2$ aqueous solution, and dried in air at room temperature. Dealumination aimed at adjusting the silicate modulus (SiO_2/Al_2O_3) of rock was carried out by modifying the samples (0,5–1 mm fraction) with a 5 mol/L HCl solution according to [35]. The degree of dealumination determined by chemical analysis has amounted to 40%.

Catalysts obtained from the above components are listed in Table 1. The L-series samples are catalytic systems consisting of separate layers of the MFI- and MOR-components with a fractional composition of 0.063-0.1 mm. The samples of C-series are composite catalytic systems with isotropic component distribution prepared by mechanical mixing. To do this, the MFI- and MOR-components were thoroughly grinded in an agate mortar in a 1 : 1 ratio, pressed and crushed to a fraction of 0.063-0.1 mm. In some cases, 30 wt% α-Al_2O_3 or γ-Al_2O_3 was added to the mixture as a binder, which is indicated in the sample name as "Bα" or "Bγ", respectively. The reduction of metals in the composites was carried out in a flow of hydrogen (50 cm^3/min) at a temperature of 653 K for 6 h.

Table 1 Two-phase composite catalysts for linear hexane hydroisomerization; the number in parentheses for the L-series samples indicates the order in which the reagent enters the corresponding layer during the reaction

Catalyst	MFI-component	MOR-component	Total content of a metal component, wt%
#L1	(I)HMFI-1Pd	(II)HR	0,5Pd
#L2	(I)HMFI-1Pd	(II)HR-2Ni	0,5Pd/1Ni
#L3	(II)HMFI-1Pd	(I)HR-2Ni	0,5Pd/1Ni
#C	HMFI-1Pd	HR-2Ni	0,5Pd/1Ni
#C-Bα	HMFI-1Pd	HR-2Ni	0,35Pd/0,7Ni
#C-Bγ	HMFI-1Pd	HR-2Ni	0,35Pd/0,7Ni

2.2 Characterization

The synthetic zeolite was investigated on a D8 ADVANCE diffractometer (Bruker) in filtered (Ni) CuKα radiation (λ = 1.542 nm) in the Bragg–Brentano focusing geometry; 2θ angle range: 5–60°, step width: 0.05°, exposure: 3 s. Powder diffraction patterns of the rock-based samples were obtained on a MiniFlex600 X-ray diffractometer (Rigaku) in CuKα radiation with the step width of 0.02° in the same 2θ interval. The scan speed, accelerating voltage, and anode current were set to 5 deg/min, 40 kV, and 15 mA, respectively. Phase analysis was performed according to [36].

Micrographs of the samples were obtained using a JEM-1230 transmission electron microscope (JEOL) with a resolution of 0.2 nm at an accelerating voltage of 80 kV. Before that, the samples were suspended in water with ethyl alcohol for 20 min using an ultrasonic bath.

FTIR spectra of the catalysts in the field of framework vibrations (400–1400 cm^{-1}) were recorded on the IRAffiniti-1s Fourier spectrometer (Shimadzu) with a single-reflection ATR accessory Specac Quest GS 10,801-B. Spectra were taken relative to air.

The IR-spectra of adsorbed pyridine on the samples were obtained in the range of 1250–4000 cm^{-1} using the Spectrum One FTIR-spectrometer (Perkin–Elmer). A tablet of a sample weighing 5–7 mg and having an area of 0.64 cm^2, pressed without a binder, was loaded into the spectral cell. The sample was evacuated at a temperature of 653 K for 1 h, and the IR-spectrum was recorded. After this, pyridine was adsorbed at a temperature of 423 K for 30 min, physically adsorbed probe molecules were removed by vacuum for 30 min, and the IR-spectrum was recorded again. Pyridine was then sequentially desorbed at 523 K, 573 K, and 723 K for 30 min followed by recording the IR-spectrum at each stage.

Isotherms of low-temperature (77 K) nitrogen ad(de) sorption were measured on a NOVA 1200e automatic sorbtometer (Quantachrome Instruments) after evacuating the samples in situ at a temperature of 573 K for 3–7 h. NovaWin software was used to calculate the parameters of a porous structure of the catalysts. The zeolite specific surface area S^{BET} was calculated using the multipoint BET method in a p/p_0 range of 0.02–0.1; the specific external surface area S^t and the volume of micropores V_{micro} – by the t-method, using the de Boer equation; the specific surface area of micropores – by the formula $S_{micro} = S^{BET} - S^t$; the total pore volume V – by the volume of adsorbed nitrogen at $p/p_0 \sim 0.99$; the average pore size R – from the assumption of their cylindrical shape. The pore size distribution was determined by the DFT method using the N_2 at 77 K on silica (cylindrical pore, NLDFT equilibrium model) calculation model.

2.3 Catalyst testing

The catalytic properties of the samples in the reaction of n-hexane hydroisomerization were tested using a microcatalytic setup. The chromatographic unit of the setup consisted of a copper capillary column (50 m long and 0.20 mm in inner diameter, squalane stationary phase) and a flame ionization detector. Chromatographic peaks were recorded using a Multyspektr-1 chromatographic attachment.

A catalyst (100 mg sample weight) was loaded into the microreactor of the setup and activated in a hydrogen flow of 20 cm^3/min at 653 K for 1 h. Then the temperature in the reactor was lowered to 473 K and the reaction was carried out at atmospheric pressure by injecting 1.0 µl of n-hexane into the H_2 carrier gas using a syringe. The products of the reaction were captured at a temperature of 77 K and transferred to the chromatographic column by heat shock (~ 610 K). Analysis conditions were as follows: the temperature in the column thermostat – 323 K; hydrogen flow – 50 cm^3/min; hydrogen and air flow rates through the detector – 30 and 300 cm^3/min, respectively. After completing the analysis, the temperature was raised by 25 degrees, and the reaction was carried out again, and so on up to 623 K.

The conversion X (wt%) and selectivity for a j-product Sj (%) were calculated as:

$$X = 100 - Y_{nC6}$$

$$S_j = \frac{Y_j}{X}$$

where Y_{nC6} is the yield of unreacted n-hexane (wt%), and Y_j is the yield of j-product (wt%). The yield of hexane isomers Y_{iC6} was calculated as the sum of the yields of 2-methylpentane (2-MP), 3-methylpentane (3-MP) and dimethylbutanes

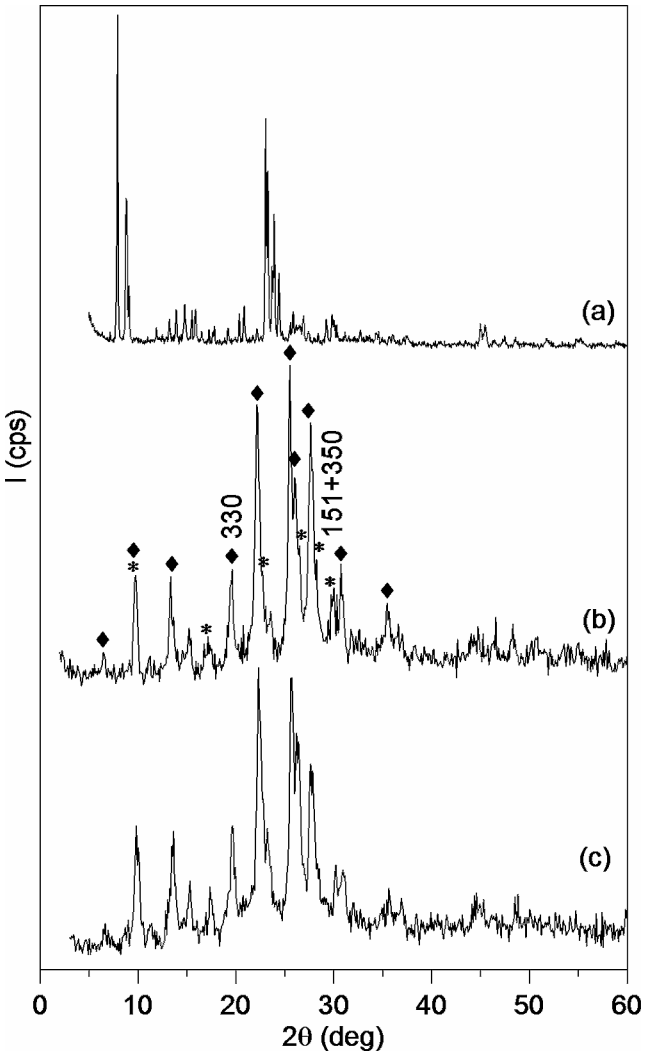

Fig. 1 Powder diffraction patterns of zeolite components of composite catalysts: (**a**) HMFI, (**b**) original rock, (**c**) dealuminated rock; ♦ – mordenite phase, * – clinoptilolite phase

(DMB). The yield of cracking products Y_{C1-5} was calculated as the sum of the yields of methane, ethane, propane, isobutane, butane, isopentane, and pentane.

3 Results and discussion

3.1 Characteristics of initial zeolite materials

Figure 1 represents the powder diffraction patterns of the zeolite components of the composites. The diffractogram of the MFI-component (Fig. 1a) contains only maxima characteristic for this type of zeolite, while the MOR-component consists of the mordenite phase as well as the clinoptilolite phase with the predominance of the former (Fig. 1b). In the acid-modified rock (Fig. 1c), the crystallinity of the mordenite phase remains intact, whereas the degree of crystallinity of the clinoptilolite phase decreases slightly and amounts to 73% of that in original rock. The degree of crystallinity has been evaluated by the relative intensity of the analytical diffraction maxima I_{330} (d = 0.453 nm) and $I_{151+350}$ (d = 0.297 nm) for mordenite and clinoptilolite, respectively. It can be assumed that partial destruction of clinoptilolite may contribute to the formation of mesoporosity in the MOR-component.

Micrographs of the components for the composites (Fig. 2) indicate the formation of nanosized particles of the metal phase. The Pd-impregnated MFI-component contains nanoparticles with a size of 7–12 nm, while in the MOR-component, Ni nanoparticles with an average size of ~ 5 nm were recorded.

The infrared spectra of the MFI and MOR-components of composite catalysts in the region of framework vibrations are shown in Fig. 3. Assignments of the main absorption bands (a.b.) are made according [37, 38]: 420 cm^{-1} – O – T – O bending vibration (T = Si, Al), 550–580 cm^{-1} – vibrations of secondary building units (SBU), 690 and 790–800 cm^{-1} – symmetric stretching internal and external vibrations of tetrahedra, respectively, 1025–1060 cm^{-1} – asymmetric stretching vibrations of bonds of tetrahedra,

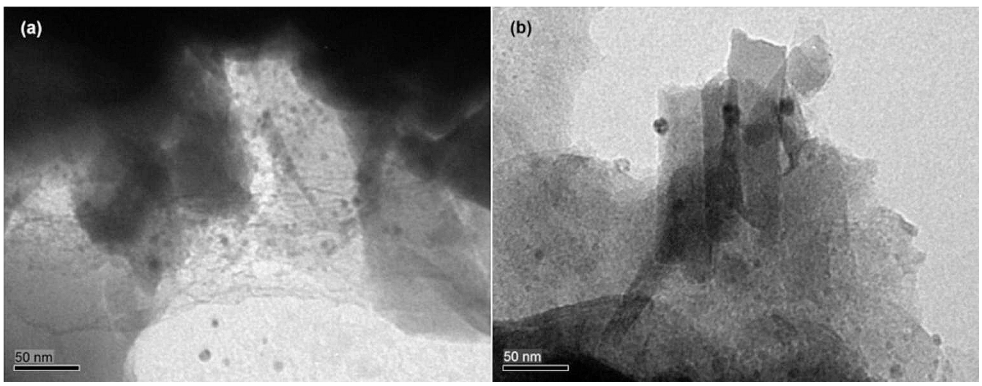

Fig. 2 TEM micrographs of the metal containing components of zeolite composites: (**a**) HMFI-1Pd, (**b**) HR-2Ni

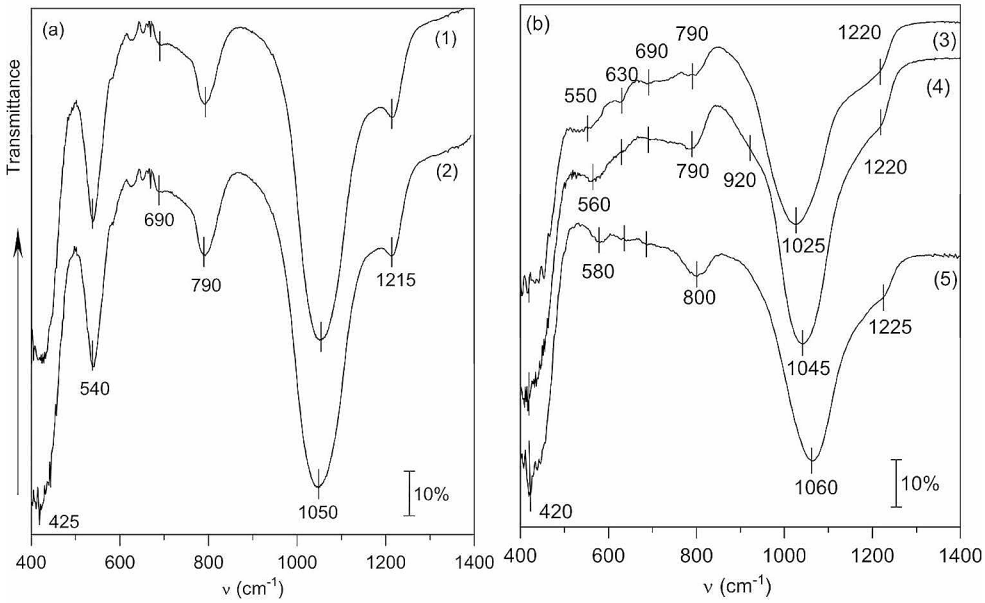

Fig. 3 FTIR spectra (**a**) MFI- and (**b**) MOR-components of composite catalysts in the region of framework vibrations: (1) HMFI, (2) HMFI-1Pd, (3) original rock, (4) dealuminated rock, (5) HR-2Ni

1220–1225 cm^{-1} – asymmetric stretching vibrations of external bonds between tetrahedra.

Spectra of the samples based on MFI zeolite (Fig. 3a) are not affected by the modification procedure: all a.b. characteristic of the zeolite are well defined, retain their position in the spectra, and their intensity remains unchanged.

As in the case of synthetic MFI-based samples, the spectra of samples of natural origin (Fig. 3b), both initial and modified, contain all characteristic a.b., the intensities of which remain intact. Thus, we can speak about the preservation, on the whole, of the crystalline structure of the rock components. However, in the spectrum of dealuminated rock, the appearance of a shoulder at 920 cm^{-1} is observed, which is often associated with various types of structural defects [39]. This indicates insignificant amorphization of the sample, which is apparently due to the partial destruction of the clinoptilolite phase during the dealumination. Dealumination also causes a high-frequency shift of the a.b. at 1025 cm^{-1} in modified samples.

In the spectrum of original rock, a broadened a.b. at 550 cm^{-1} is observed, which narrows and shifts in the modified samples. The same was observed for another rock by Voloshyna et al. [40] and explained by the diversity of cationic composition of native rock and its homogeneity in the H-form of samples. The effect of cationic composition on the frequency of SBU vibrations in mordenite and clinoptilolite can be noticeable due to the high concentration of cationic sites in their free space. On the other hand, metal particles in the zero-valent state can also affect the SBU vibrations, restricting their motion, which leads to a high-frequency shift of this a.b. in the spectrum of the HR-2Ni sample.

3.2 Porous structure and acidity characteristics of initial materials and composite systems

The porous structure of the samples was estimated from the isotherms of low-temperature nitrogen ad(de)sorption (Fig. 4).

The shape of the isotherm of the MFI-based samples is typical for microporous adsorbents according to the IUPAC classification [41]. The proportion of micropores in these samples is > 80% (Table 2). A minor hysteresis is observed on the isotherms, the occurrence of which is explained by the slight destruction of the porous structure during the obtaining of the protonic form.

The isotherms of the rock-based samples have a character intrinsic to sorbents that combine micro- and mesoporosity. This is evidenced by a sharp rise at low relative pressures and the presence of a hysteresis loop at higher p/p_0, respectively. The proportion of micropores in these samples is about 55%. The reason for the appearance of hysteresis with a pronounced rise in the region of high relative pressures is obviously the appearance of mesopores inside the crystallites during the dealumination procedure due to partial destruction of the structure.

The pore size distribution (Fig. 5) for the zeolite samples has three maxima: about 1 nm, 1.2 nm, and 2.6 nm. Accordingly, one can distinguish pores with a radius of 1 nm, which are classified as supermicropores [41] and predominate in the MFI-based samples, as well as narrow mesopores with a radius of about 1.2 nm, which predominate in the rock-based samples. The volume of mesopores with a radius of 2.6 nm is insignificant in both zeolites. Therefore, the

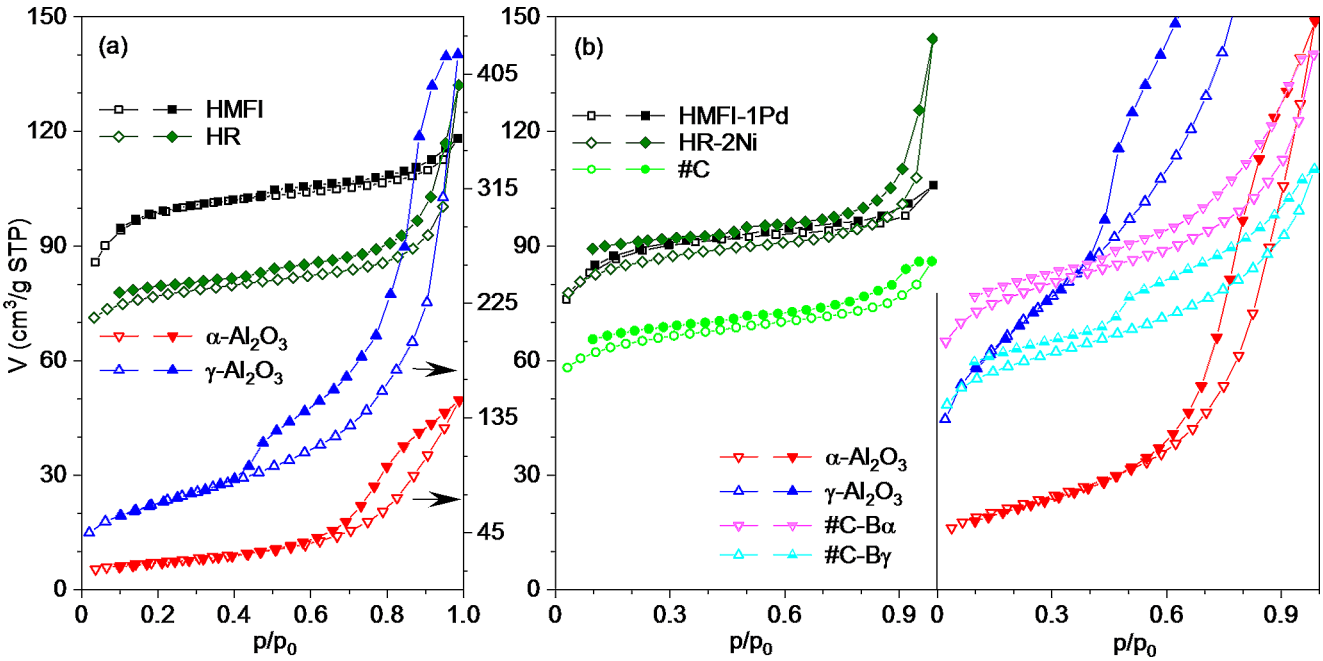

Fig. 4 N_2 ad(de)sorption isotherms (T = 77 K) of (**a**) the initial materials, (**b**) the composite catalysts and their components apart, with a recovered metal component; blank symbols – adsorption, filled symbols – desorption

Table 2 Porous structure parameters of the samples

Samples	S^{BET} (m^2/g)	S^t (m^2/g)	S_{micro} (m^2/g)	V_{micro} (cm^3/g)	V (cm^3/g)	V_{micro}/V (%)	R(nm)	R^{DFT} (nm)
MFI-based								
HMFI	371	14.5	356	0.150	0.183	82	0.99	0.97
HMFI-1Pd	332	11.3	321	0.136	0.164	83	0.99	0.97
Rock-based								
HR	345[a)]	19.1	326	0.113	0.205	55	1.38	1.17
HR-2Ni	330	19.3	310	0.126	0.223	57	1.35	1.17
Binder								
α	78.3	66.9	11.4	0.005	0.230	2.0	5.88	4.56
γ	243	211	32.7	0.013	0.651	2.0	5.35	2.55
Composite catalytic system								
#C	247	15.6	232	0.097	0.133	73	1.08	1.17
#C-Bα	291	56.9	234	0.096	0.217	44	1.49	1.13
#C-Bγ	219	53.2	165	0.071	0.170	42	1.56	1.17

[a)]The specific surface area for this sample was calculated using the Langmuir equation

secondary porosity of both zeolite components can be considered similar.

As a result of modification with metals, the parameters of the porous structure of the samples decrease compared to the original materials. At the same time, a decrease in the specific surface area of the HR-2Ni sample is accompanied by an increase in the volume of micropores and the volume of pores with a radius of ~ 1.2 nm prevailing in the rock. In this case, this increase may be imaginary and can be explained by an increase in the amount of adsorption under the influence of nickel particles, which serve as additional adsorption sites. Palladium atoms, due to their larger radius, have greater polarizability, which leads to a stronger van der Waals interaction of palladium particles with the zeolite surface [42]. Therefore, for nitrogen molecules, they are unlikely to create additional adsorption sites. For this reason, the calculation of the pore volume from the N_2 adsorption isotherms in the case of palladium seems to be more adequate. The above mentioned indicates the location of metal particles in the nanopores that predominate in a particular zeolite, but in the rock-based samples, nickel is also present in zeolite micropores.

Both modifications of aluminum oxide, which were used as binders in the preparation of samples #C-Bα and #C-Bγ, show isotherms with a wide hysteresis loop. They are characteristic of mesoporous adsorbents with a small number

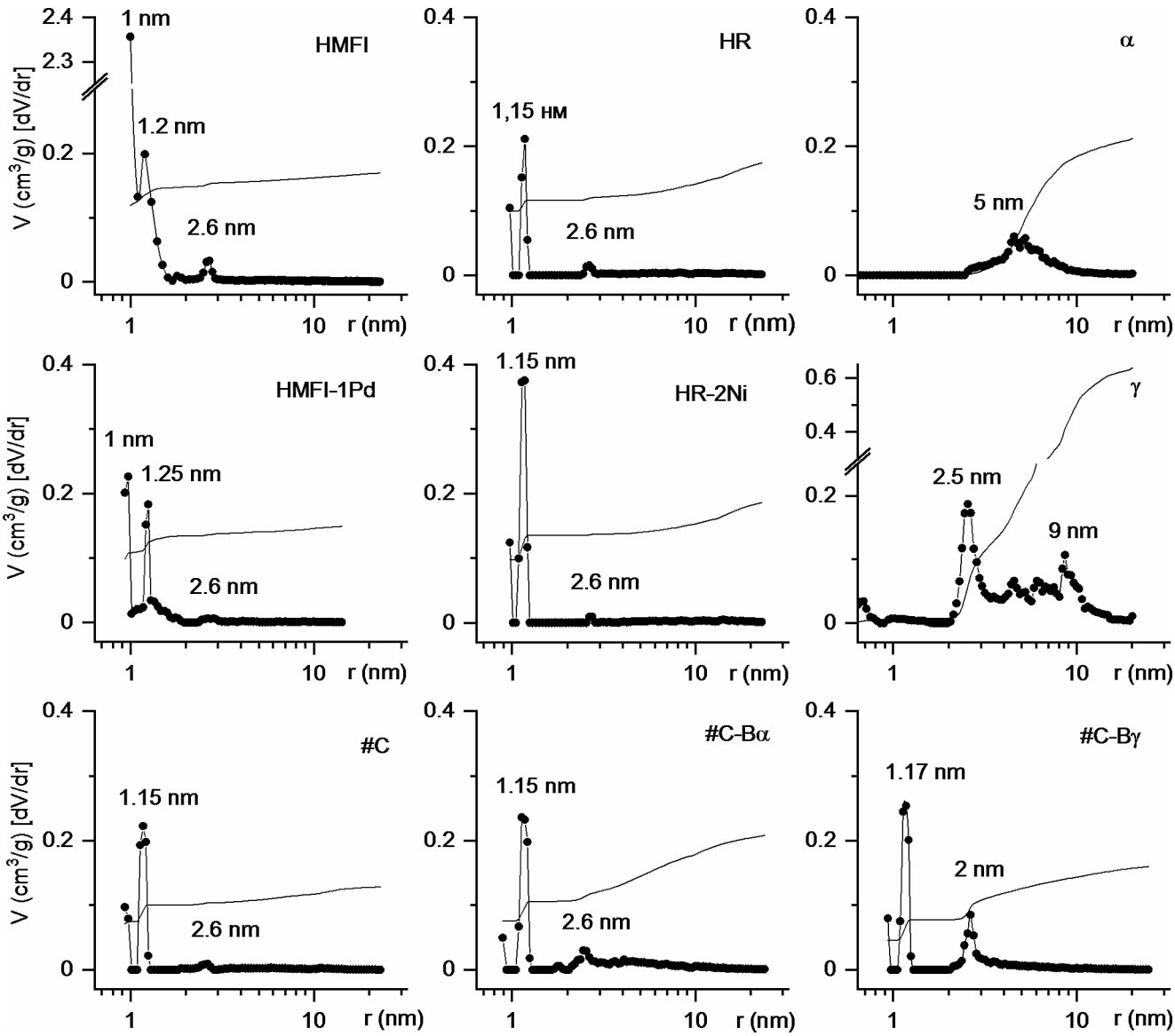

Fig. 5 Pore size distribution and cumulative pore volume (DFT) based on low-temperature N_2 ad(de)sorption data

of micropores. γ-Al_2O_3 has a threefold higher specific surface area compared to α-Al_2O_3. The average pore radius for these samples is 5–6 nm. Pores size distribution gives a wide maximum near 5 nm for α-Al_2O_3, and for γ-Al_2O_3 – a dispersion of radii in the range of 2–10 nm with a predominance of 2.5 nm radius.

Interestingly, the composite catalyst #C has worse porosity parameters than its components. The addition of a binder in the #C-Bα sample is reflected in a significant increase in the external surface area and total pore volume. The latter increases due to the addition of nanopores with radii of 2–10 nm to the porous structure (Fig. 5). In the #C-Bγ sample, the size distribution of nanopores resulting from the addition of the binder is much narrower with a maximum of about 2 nm. The larger pores present in γ-Al_2O_3 are obviously formed by the inter-particle space that is destroyed during the mixing process. With that, γ-Al_2O_3 loses a significant portion of its pore volume, which is not the case with α-Al_2O_3 when added to a mixture of zeolites. The observed phenomenon is explained, on the one hand, by the much higher dispersion of γ-Al_2O_3 compared to the dispersion of zeolite components of the composites and, on the other hand, by the close particle sizes of zeolites and α-Al_2O_3 [43]. The former is also the reason for the somewhat reduced micropore surface area of the #C-Bγ composite, which is due to the blockage of pore openings on the external surface of zeolite crystallites.

The acidity of the samples was evaluated by means of FTIR spectroscopy using pyridine as a probe molecule. The spectra contain characteristic a.b. related to pyridine

coordinated at Lewis acid sites (LAS) and pyridine protonated at Brønsted acid sites (BAS), 1450–1462 cm^{-1} and 1545 cm^{-1}, respectively (Fig. 6a). As the temperature of evacuation increases, the intensity of LAS a.b. gradually increases. A high-frequency shift for these a.b. is simultaneously observed. This indicates a decrease in the number of stronger LAS capable of coordinating pyridine at higher temperatures. On the contrary, BAS a.b. are more stable: their intensity decreases noticeably only after evacuation at 723 K, except for the HR-2Ni sample, which indicates the presence of strong BAS in the composite catalysts. As for HR-2Ni, a considerable part of BAS-protonated pyridine as well as LAS-coordinated pyridine is desorbed already at 423 K. This demonstrates that this catalyst contains weakly and moderately strong acid sites of both types. Their concentration is lower than in the composite catalyst #C, which includes a Pd-containing MFI-component (Fig. 6b). Taking into account that in these two catalysts Lewis acidity is introduced mainly by the metal component, the observed increase in the concentration of acid sites in the catalyst #C can be explained by the effect of Pd on the state of Ni (its dispersity, reducibility, etc.) [44]. The ratio of BAS to LAS for #C is the highest among the studied samples. The addition of binder results in a threefold decrease in the BAS/LAS ratio for #C-Bα and #C-Bγ due to the Lewis nature of the acidity of α- and γ-Al_2O_3.

3.3 Catalysis

The catalysts were tested in the isomerization of linear hexane in a micro-pulse mode, and the activity was evaluated by the degree of conversion of the reagent.

The conversion of n-hexane on catalysts of the L-series, in which the zeolite components are separate layers, begins at 473 K (Fig. 7a). The lowest conversion is observed for the monometallic sample #L1, but thanks to Pd it is the most selective for C_6 isomers (Fig. 7b). With increasing temperature, the isomerization selectivity on all three catalysts decreases. The addition of Ni to the MOR component (samples #L2 and #L3) obviously promotes the activation of cracking, which is reflected in the increase in conversion over these samples comparing to the #L1 sample and, accordingly, a decrease in their selectivity. In addition, there is a tendency to decrease the temperature of the maximum

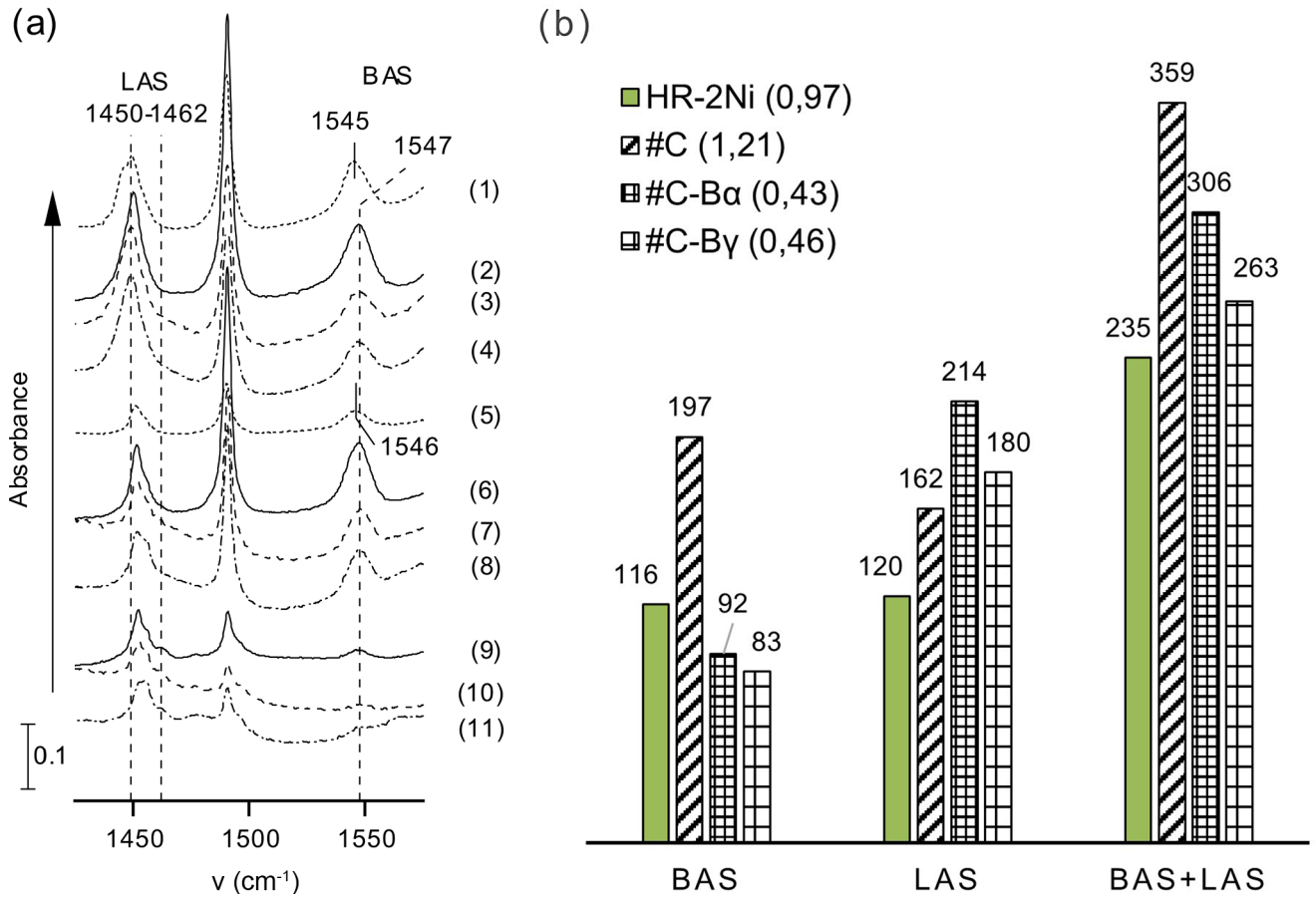

Fig. 6 (**a**) FTIR spectra of adsorbed pyridine on samples of the catalysts HR-2Ni (1, 5), #C (2, 6, 9), #C-Bα (3, 7, 10), and #C-Bγ (4, 8, 11) after evacuation at 423 K (1–4), 523 K (5), 573 K (6–8), and 723 K (9–11); (**b**) acid site distribution in the samples (in parentheses, a ratio of BAS to LAS is noted) calculated according to [45] from the amount of pyridine adsorbed at 423 K

yield of hexane isomers (Fig. 7c) without reducing the maximum value. The effect of the addition of nickel differs depending on which catalyst layer is first exposed to hexane. Since the #L2 catalyst, which has a Pd-containing layer first, is more efficient than the other Ni-containing catalyst in this series, it can be assumed that the role of palladium is to provide initial effective dehydrogenation of alkanes, which facilitates further isomerization. Hydrogenation of the formed isomers to the final products can occur on less effective hydrogenating-dehydrogenating sites, such as nickel nanoparticles. This approach provides a basis for minimizing the content of expensive metals in composite catalysts.

As can be seen from Fig. 7c, d on the example of the formation of hexane isomers, the total effect of the two layers is not additive and exceeds their average value.

To further determine the effect of the arrangement of catalyst layers on the hexane transformation, samples #C, #C-Bα and #C-Bγ with an isotropic distribution of zeolite phases were prepared and their catalytic properties were studied (Fig. 8).

First of all, it should be noted that these catalysts, with the exception of sample #C-Bγ, showed significantly better results in the isomerization of n-hexane compared to sample #L2, the most effective catalyst of the L-series. This may indicate that the above-mentioned positive effect of the initial more efficient dehydrogenation of reagent molecules on palladium can occur not only at the macro level in the case of layering of Pd- and Ni-containing components of the composite catalyst, but also under conditions of isotropic distribution of the corresponding zeolite components in the catalyst. In the latter case, it is even more effective.

As is well known, γ-Al_2O_3 is widely used as a catalyst carrier and can also serve as an active catalyst due to the presence of LAS and a developed specific surface area, while α-Al_2O_3 is characterized by an order of magnitude lower concentration of LAS on the surface [43]. At the same time, in α-oxide, LAS are weak [46] and porosity is three times less developed than in γ-Al_2O_3 (Table 2). However, the #C-Bα sample obtained using α-aluminum oxide is significantly superior in all respects to the #C-Bγ catalyst, in which γ-Al_2O_3 was used as a binder (Fig. 8). Obviously, the acidic properties of γ-Al_2O_3 are not an advantage for hydroisomerization and hydrocracking reactions, since in these reactions the active sites are above all BAS, whose concentration in the #C-Bγ is lowest among #C-series

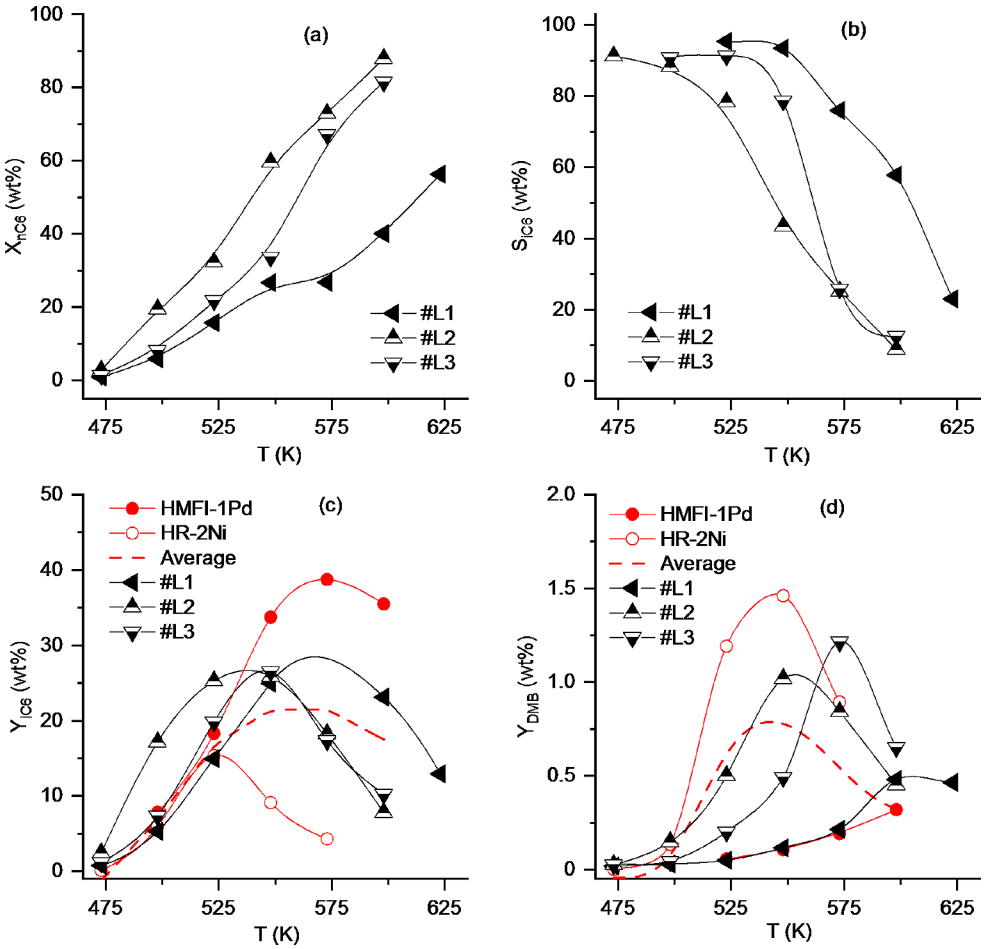

Fig. 7 (**a**) Conversion of n-hexane X_{nC6}, (**b**) selectivity for C_6 isomers S_{iC6} and (**c**) their yield Y_{iC6}, and (**d**) yield of dimethylbutanes Y_{DMB} on L-series catalysts and their zeolite components; (**c**), (**d**) a dash-line presents average yields for the MFI- and MOR-components

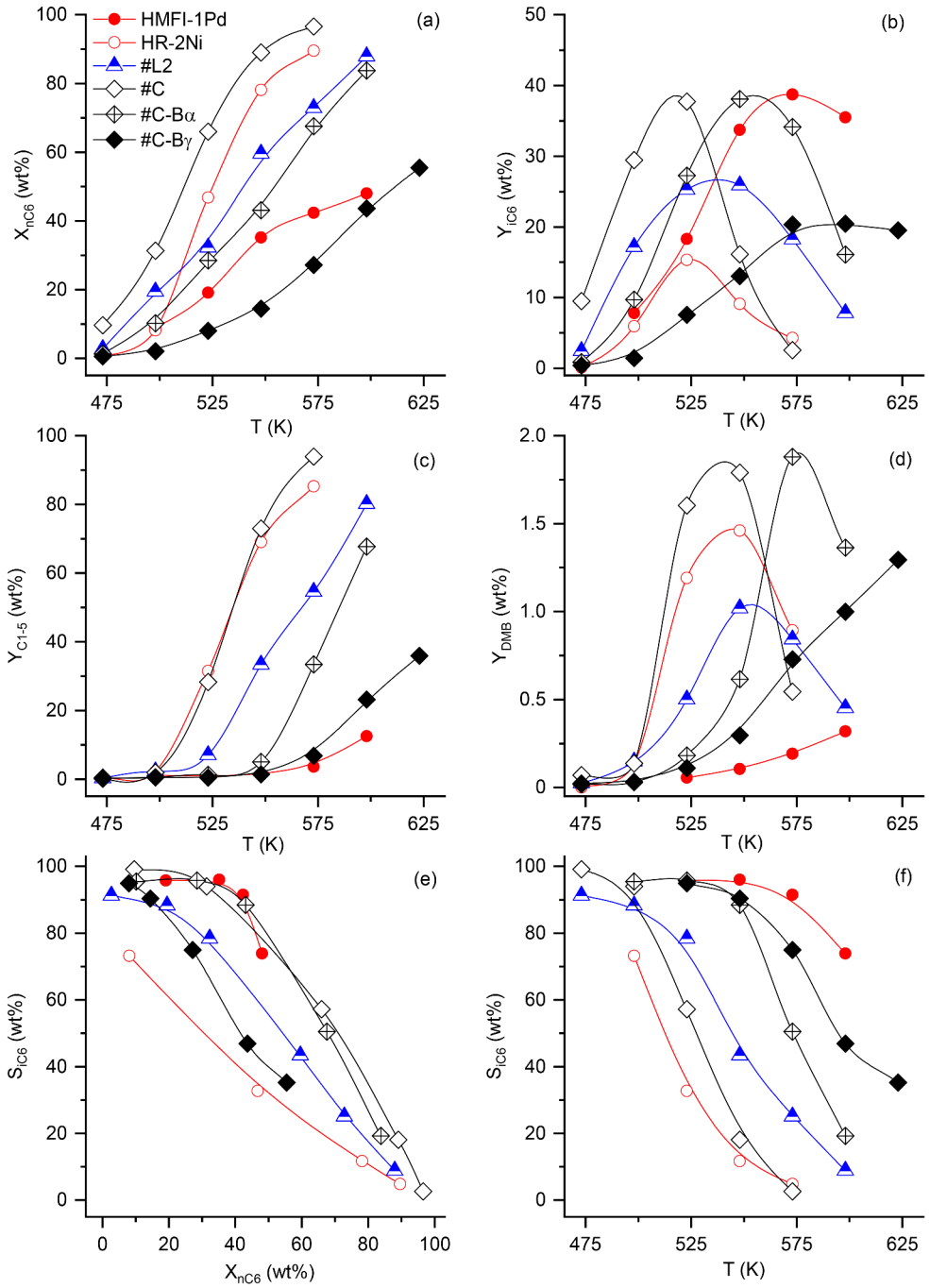

Fig. 8 (**a**) Conversion of n-hexane X_{nC6}, yields of (**b**) C_6 isomers Y_{iC6}, (**c**) cracking products Y_{C1-5} and (**d**) dimethylbutanes Y_{DMB}, as well as selectivity for C_6 isomers S_{iC6} vs (**e**) conversion X_{nC6} and (**f**) temperature T for the composite catalysts

catalysts (Fig. 6b). The advantage in porosity is also lost during the preparation of the #C-Bγ composite (see subsection 3.2). Instead, this composite has a 30% smaller micropore surface area, where the active sites are located. This reduces the degree of conversion on this catalyst, as well as its selectivity (Fig. 8e), since in the micropores isomerization would be facilitated by a longer stay of the reagents in contact with the active surface.

On the composite catalyst #C-Bα, with increasing temperature, the yield of C_6 isomers begins to increase, which at a maximum at a temperature of 548 K approaches the highest value for the tested catalysts – 40%. (Fig. 8b). Obviously, with an increase in the reaction temperature, there is a gradual increase in the strength of the BAS. At a temperature of 573 K, a sharp increase in the yield of cracking products C_{1-5} is observed (Fig. 8c), indicating the appearance of sufficiently strong sites and acceleration of the cracking reaction. On the #C-Bγ sample, these processes are much less pronounced compared to #C-Bα, which is explained by

the lower accessibility of the sites due to the blockage of micropore in this catalyst, as shown above.

The maximum yield of C_6 isomers on samples #C and #C-Bα (samples of the C-series with isotropic distribution of zeolite components, except for #C-Bγ) remains as high as on their Pd-containing component, sample HMFI-1Pd, but is observed at a lower temperature (Fig. 8b). At the same time, the yield of valuable dimethyl branched isomers on the composites increases by an order of magnitude compared to this component, exceeding the high yield of DMB on its other component, the HR-2Ni sample (Fig. 8d). Both composite catalysts, despite the lower Pd content and the presence of Ni, retain high selectivity for C_6 isomers of their Pd-containing component (Fig. 8e). It can be concluded that such factors as Ni content and the presence of a binder in the composition affect only the activity of the catalyst, as evidenced by the divergence of the curves of the temperature dependence of the selectivity. (Fig. 8f). The highest effectiveness in the formation of hexane isomers in general, as well as dimethyl branched isomers, is demonstrated by sample #C, obtained without the use of a binder. Considering its acidic characteristics, it can be stated that the maximum concentration of Brønsted acid sites and the highest BAS to LAS ratio among the composites studied contribute to this. This catalyst in terms of the iC_6 yield is close to the bimetallic monozeolite catalyst with a similar cationic composition (0.5 wt% Ni and 0.5 wt% Pd, [33]), but, unlike the composite, the latter almost does not form DMB.

4 Conclusions

Composite catalytic systems with separated zeolite phases were prepared by mechanical mixing (1:1), optionally with the addition of a binder. They included the synthetic MFI zeolite component, the natural mordenite component, and hydrogenating-dehydrogenating metal component. The MFI-component contained Pd nanoparticles with a size of 7–12 nm, and Ni nanoparticles with an average size of ~5 nm were formed in the MOR-component. The MFI-component of the catalysts had a microporous structure, and the MOR-component was micro-mesoporous due to partial destruction of the clinoptilolite phase of rock. The use of a binder significantly increased the external surface of the catalysts and contributed to the appearance of nanosized pores with a radius of 2–10 nm. The composite obtained without a binder remained mostly microporous.

Different modifications of aluminum oxide, when used as a binder, affect differently the effectiveness of the obtained catalytic systems in the conversion of n-hexane. This is explained by the different dispersity of α- and γ-Al_2O_3 particles, which causes differences in the characteristics of the porous structure of the obtained composites and, in turn, different accessibility of their active sites. In this respect, α-Al_2O_3 is more favorable than γ-Al_2O_3.

It was found that the catalytic behavior of composites with separated zeolite phases is not only determined by their porosity. The highest effectiveness in the formation of hexane isomers in general, as well as dimethyl branched isomers, is demonstrated by the sample possess the maximum concentration of Brønsted acid sites and the highest BAS to LAS ratio.

The results obtained indicate that studied composite catalytic systems are promising for use as catalysts for the hydroisomerization of linear alkanes. Synergy between the two zeolite components in the formation of hexane isomers is observed for the obtained composites. This effect is explained by the productive mutual influence of metal phases included in the zeolite. The synergy is more effective in the case of an isotropic distribution of zeolite phases. The catalysts demonstrate selectivity for n-hexane isomers at the level of high selectivity of the Pd-containing component, having higher effectiveness in the formation of hexane isomers in general, as well as valuable dimethyl-branched isomers.

Acknowledgements The authors are grateful to O.V. Shvets (L.V. Pysarzhevskyi Institute of Physical Chemistry, National Academy of Sciences of Ukraine) and M.M. Filonenko (University of State Fiscal Service of Ukraine) for their help in obtaining the powder diffraction patterns of the samples, M.M. Kurmach (L.V. Pysarzhevskyi Institute of Physical Chemistry, National Academy of Sciences of Ukraine) for the help in obtaining IR spectra of adsorbed pyridine on the samples, and S.M. Shcherbakov (M.G. Kholodny Institute of Botany, National Academy of Sciences of Ukraine) for assistance in obtaining the micrographs of the samples. The authors also express their gratitude to the European Chemistry School for Ukrainian (https://ecpsfu.org) for providing an overview of current trends in European chemical science.

Author contributions Conceptualization: L.K.P.; Methodology: Y.G.V., O.P.P.; Investigation: O.P.P., A.V.Y., V.A.P.; Validation: O.P.P., A.V.Y.; Formal analysis: Y.G.V., O.P.P.; Data Curation: Y.G.V.; Resources: V.A.P.; Writing and visualization: Y.G.V. All authors reviewed and approved the manuscript.

Funding No funding was received for conducting this study.

Data availability No datasets were generated or analysed during the current study.

Declarations

Competing interests The authors declare no competing interests.

References

1. Z. Liu, Y. Wang, Z. Xie, Chin. J. Catal. **33**, 22–38 (2012). https://doi.org/10.1016/s1872-2067(10)60299-9

2. X. Qi, B. Li, S. Li, X. Liu, B. Lin, Chin. J. Catal. **27**, 228–232 (2006)
3. Z. Xie, Z. Liu, Y. Wang, Q. Yang, L. Xu, W. Ding, Int. J. Mol. Sci. **11**, 2152–2187 (2010). https://doi.org/10.3390/ijms11052152
4. M.S. Francesconi, Z.E. Lopez, D. Uzcategui, G. Gonzalez, J.C. Hernandez, A. Uzcategui, A. Loaiza, F.E. Imbert, Catal. Today. **107–108**, 809–815 (2005). https://doi.org/10.1016/j.cattod.2005.07.013
5. X.L. Niu, Y.Q. Song, S.J. Xie, S.L. Liu, Q.X. Wang, L.Y. Xu, Catal. Lett. **103**, 211–218 (2005). https://doi.org/10.1007/s10562-005-7156-4
6. S. Xie, S. Liu, Y. Liu, X. Li, W. Zhang, L. Xu, Microporous Mesoporous Mater. **121**, 166–172 (2009). https://doi.org/10.1016/j.micromeso.2009.01.027
7. H. Chen, B. Shen, H. Pan, Chem. Lett. **32**, 726–727 (2003). https://doi.org/10.1246/cl.2003.726
8. A.S. Kovo, E. Opuama, M.O. Edoga, M. Abdulkadir, A.G. Isah, I.A. Mohammed, Chem. Eng. Sci. **4**, 1–4 (2016). https://doi.org/10.12691/ces-4-1-1
9. Y.-H. Kang, X.-Y. Wei, G.-H. Liu, Y. Gao, Y.-J. Li, X.-R. Ma, Z.-F. Zhang, Z.-M. Zong, Fuel. **269**, 117326 (2020). https://doi.org/10.1016/j.fuel.2020.117326
10. A.A. Al-Shammari, S.A. Ali, N. Al-Yassir, A.M. Aitani, K.E. Ogunronbi, K.A. Al-Majnouni, S.S. Al-Khattaf, Fuel Process. Technol. 122, 12–22 (2014) https://doi.org/10.1016/j.fuproc.2014.01.021
11. L. Li, X. Cui, J. Li, J. Wang, J. Braz Chem. Soc. **26**, 290–296 (2015). https://doi.org/10.5935/0103-5053.20140279
12. Y. Ghrib, N. Frini-Srasra, E. Srasra, J. Martínez-Triguero, A. Corma, Catal. Sci. Technol. **8**, 716–725 (2018). https://doi.org/10.1039/C7CY01477E
13. Q.Q. Zhao, B. Qin, J.J. Zheng, Y.Z. Du, W.F. Sun, F.X. Ling et al., Chem. Eng. J. **257**, 262–272 (2014). https://doi.org/10.1016/j.cej.2014.07.056
14. X. Dai, X. Qi, Y. Guo, D. Kong, Chem. Reaction Eng. Technol. **27**, 385–392 (2011)
15. D.J. Kong, J.L. Zheng, X.H. Yuan, Y.D. Wang, D.Y. Fang, Microporous Mesoporous Mater. **119**, 91–96 (2009). https://doi.org/10.1016/j.micromeso.2008.10.001
16. X. Chen, Chem. Reaction Eng. Technol. **34**, 36–42 (2018). https://doi.org/10.11730/j.issn.1001-7631.2018.01.0036.07
17. L. Zhang, Z.-X. Jiang, Y. Yu, C.-S. Sun, Y.-J. Wang, H.-Y. Wang, RSC Adv. **5**, 55825–55831 (2015). https://doi.org/10.1039/c5ra10296k
18. R. Zhang, J. Wang, L. Han, J. Wang, L. Zhao, J. Phys. Chem. Solids. **157**, 110194 (2021). https://doi.org/10.1016/j.jpcs.2021.110194
19. X. Wang, S. Guo, Z. Niu, RSC Adv. **13**, 2081–2089 (2023). https://doi.org/10.1039/D2RA07499K
20. T. Sontisawate, H. Nasu, T. Hashimoto, A. Ishihara, J. Jpn Petrol. Inst. **59**, 184–196 (2016). https://doi.org/10.1627/jpi.59.184
21. Z.S. Qureshi, M.A. Siddiqui, A. Tanimu, A. Aitani, A.C. Akah, Q. Xu, M. AlHerz, J. Anal. Appl. Pyrol. **166**, 105621 (2022). https://doi.org/10.1016/j.jaap.2022.105621
22. A. Bordoloi, B.M. Devassy, P.S. Niphadkar, P.N. Joshi, S.B. Halligudi, J. Mol. Catal. A: Chem. **253**, 239–244 (2006). https://doi.org/10.1016/j.molcata.2006.03.045
23. S.A. Ali, F.M. Almulla, B.R. Jermy, A.M. Aitani, R.H. Abudawoud, M. AlAmer, Z.S. Qureshi, T. Mohammad, H.S. Alasiri, J. Ind. Eng. Chem. **98**, 189–199 (2021). https://doi.org/10.1016/j.jiec.2021.04.003
24. V.S.P. Ganjala, C.K.P. Neeli, C.V. Pramod, M. Khagga, K.S.R. Rao, D.R. Burri, Catal. Commun. **49**, 82–86 (2014). https://doi.org/10.1016/j.catcom.2014.02.006
25. M. Fedyna, A. Żak, K. Jaroszewska, J. Mokrzycki, J. Trawczyński, Microporous Mesoporous Mater. **305**, 110366 (2020). https://doi.org/10.1016/j.micromeso.2020.110366
26. K. Okada, Y. Kameshima, C.D. Madhusoodana, R.N. Das, Sci. Technol. Adv. Mater. **5**, 479–484 (2004). https://doi.org/10.1016/j.stam.2004.03.001
27. H. Katsuki, S. Furuta, S. Komarneni, J. Am. Ceram. Soc. **83**, 1093–1097 (2004). https://doi.org/10.1111/J.1151-2916.2000.TB01336.X
28. L. Patrylak, R. Likhnyovskyi, V. Vypyraylenko, R. Leboda, J. Skubiszewska-Zięba, K. Patrylak, Adsorp Sci. Technol. **19**, 525–540 (2001). https://doi.org/10.1260/0263617011494376
29. L.K. Patrylak, S.V. Konovalov, A.V. Yakovenko, O.P. Pertko, V.A. Povazhnyi, Y.G. Voloshyna, O.V. Melnychuk, M.M. Filonenko, Appl. Nanosci. **13**, 4795–4808 (2023). https://doi.org/10.1007/s13204-022-02620-5
30. M.R. Abukhadra, S.M. Ibrahim, S.M. Yakout, M.E. El-Zaidy, A.A. Abdeltawab, Energy Convers. Manag. **196**, 739–750 (2019). https://doi.org/10.1016/j.enconman.2019.06.027
31. M.M. Kurmach, K.M. Konysheva, K.O. Filatova, S.O. Sotnik, K.S. Gavrilenko, O.V. Andreev, O.V. Shvets, Theor. Exp. Chem. **57**, 451–457 (2022). https://doi.org/10.1007/s11237-022-09715-8
32. L.K. Patrylak, M.M. Krylova, O.P. Pertko, Y.G. Voloshyna, J. Porous Mater. **26**, 861–868 (2019). https://doi.org/10.1007/s10934-018-0685-1
33. L. Patrylak, O. Pertko, Y. Voloshyna, A. Yakovenko, V. Povazhnyi, O. Melnychuk, K. Zlochevskyi, Chem. Chem. Technol. **15**, 330–335 (2021). https://doi.org/10.23939/chcht15.03.330
34. Y.G. Voloshyna, O.P. Pertko, L.K. Patrylak, A.V. Yakovenko, Vopr Khimii i Khimicheskoi Tekhnologii. **6**, 26–32 (2020). https://doi.org/10.32434/0321-4095-2020-133-6-26-32. [in Ukrainian]
35. Y.G. Voloshyna, O.P. Pertko, V.A. Povazhnyi, L.K. Patrylak, A.V. Yakovenko, Appl. Nanosci. **13**, 4863–4872 (2023). https://doi.org/10.1007/s13204-022-02632-1
36. IZA Structure Commission, Database of Zeolite Structures. (editing status: fully revised 2017), http://www.iza-structure.org/databases/. Accessed 21 Dec 2023
37. F. Pechar, D. Rykl, Chem. Zvesti. **35**, 189–202 (1981)
38. J.C. Jansen, F.J. van der Gaag, H. van Bekkum, Zeolites. **4**, 369–372 (1984). https://doi.org/10.1016/0144-2449(84)90013-7
39. S. Bordiga, C. Lamberti, F. Bonino, A. Travert, F. Thibault-Starzyk, Chem. Soc. Rev. **44**, 7262–7341 (2015). https://doi.org/10.1039/C5CS00396B
40. Y. Voloshyna, O. Pertko, V. Povazhnyi, L. Patrylak, A. Yakovenko, Chem. Chem. Technol. **17**, 373–385 (2023). https://doi.org/10.23939/chcht17.02.373
41. M. Thommes, K. Kaneko, A.V. Neimark, J.P. Olivier, F. Rodriguez-Reinoso, J. Rouquerol, K.S.W. Sing, Pure Appl. Chem. **87**, 1051–1069 (2015). https://doi.org/10.1515/pac-2014-1117
42. J. Kim, S.W. Han, J.-C. Kim, R. Ryoo, ACS Catal. **8**, 10545–10554 (2018). https://doi.org/10.1021/acscatal.8b03301
43. S. Kiatphuengporn, A. Junkaew, C. Luadthong, S. Thongratkaew, C. Yimsukanan, S. Songtawee, T. Butburee, P. Khemthong, S. Namuangruk, M. Kunaseth, K. Faungnawakij, Green. Chem. **22**, 8572–8583 (2020). https://doi.org/10.1039/D0GC02573A
44. S.A. Karakoulia, E. Heracleous, A.A. Lappas, Catal. Today. **355**, 746–756 (2020). https://doi.org/10.1016/j.cattod.2019.04.072
45. C.A. Emeis, J. Catal. **141**, 347–354 (1993). https://doi.org/10.1006/jcat.1993.1145
46. A. Zecchina, S. Bordiga, G. Spoto, D. Scarano, G. Petrini, G. Leofanti, M. Padovan, C.O. Areàn, J. Chem. Soc. Faraday Trans. **88**, 2959–2969 (1992). https://doi.org/10.1039/FT9928802959